$5f$-electron localization in uranium binary hydrides: Photoelectron spectroscopy

Oleksandra Koloskova,[1] Banhi Chatterjee,[2] Ladislav Havela,[1,*] Thomas Gouder,[3] and Jindřich Kolorenč[4,†]

[1]*Department of Condensed Matter Physics, Faculty of Mathematics and Physics, Charles University, Ke Karlovu 3, 121 16 Prague 2, Czech Republic*

[2]*Jožef Stefan Institute, Jamova 39, SI-1000 Ljubljana, Slovenia*

[3]*European Commission, Joint Research Centre (JRC), Postfach 2340, D-76125 Karlsruhe, Germany*

[4]*Institute of Physics (FZU), Czech Academy of Sciences, Na Slovance 2, 182 00 Prague, Czech Republic*

(Received 13 July 2023; revised 21 December 2023; accepted 2 February 2024; published 27 February 2024)

The relation of $5f$-electron localization and valence-band x-ray and ultraviolet photoelectron spectra (XPS, UPS) is analyzed on the example of uranium binary hydrides UH_3 and UH_2. Confronted with results of density functional theory (DFT) and DFT + U calculations, it is recognized that electron-electron correlations play an important role. The spectra can be well accounted for by dynamical mean-field theory (DMFT) calculations providing insight into the final state remaining after the photoexcitation event. It is concluded that details of the spectra reflect the dominant final-state $5f^2$ multiplets with the main line $^3H_4$ adjacent to the Fermi level and the first excited line $^3F_2$ responsible for a shoulder at 0.5 eV binding energy. Calculations with a varied strength of hybridization between $5f$ and non-f states allow us to visualize how the individual multiplet lines shift in energy. The one-to-one correspondence between features seen in the DMFT calculations and free-ion multiplets remains noticeable even with the realistic strength of the hybridization included, but the positions of some of the lines can vary substantially. The width of the distribution characterizing fluctuations of the $5f$ filling among the individual integral $5f^N$ states, approximated by a Gaussian distribution with a certain width, is suggested as a quantification of the $5f$ delocalization. In this respect, the hydrides are found to be more delocalized than UGa_2 or δ-Pu.

DOI: 10.1103/PhysRevB.109.075165

I. INTRODUCTION

Open $5f$ electronic shells in actinide systems are responsible for diverse exotic phenomena, such as unconventional superconductivity in UTe_2 [1] or $PuCoGa_5$ [2], hidden-order state in URu_2Si_2 [3], or heavy-fermion magnetic (U_2Zn_{17} [4]) or nonmagnetic (UBe_{13} [5]) systems. The main ingredients responsible for these phenomena are undoubtedly the variable degree of itinerancy, electron-electron correlations, and very strong spin-orbit interaction, bringing large orbital moments into states involved in and affected by metal bonding.

Although a lot of attention has been paid to a handful of truly exotic compounds, it is important to look at the workings of the same mechanisms, delocalization, electron-electron correlations, and spin-orbit interaction in more simple cases, where a general understanding should be easier to reach, and in which the attributes of the incipient Mott transition (taking place between Pu and Am in pure elements) can be systematically traced in bulk and microscopic experimental data. One of the issues is to reconcile our perception of the electronic structure with the results of electron spectroscopies, which proved to be absolutely essential to identify that Pu metal is not a simple band system, which would be nonmagnetic because the Pu-Pu distances are too short. In particular, photoelectron spectroscopy appeared as an indicator of the involvement of the nonmagnetic $5f^6$ state, yielding the $5f^5$-$5f^6$ fluctuations eventually suppressing the magnetism of the $5f^5$ shell [6,7]. Dynamical mean-field theory (DMFT) computations then provide access even to the low-energy scale, revealing strong enhancement of the Sommerfeld coefficient of the electronic specific heat [8].

While the Pu problem has been at least qualitatively resolved, the difficulties remain in systems of lighter actinides, having a tendency to more delocalized $5f$ states, which, in addition, yield magnetic ground state unless the $5f$ band is too broadened due to very short U-U spacings [9]. A simple ferromagnetism with large uranium magnetic moments is quite common in uranium binary systems. One example, which does not contain any transition metal and the consequent $5f$-d interaction that would bring additional degrees of freedom, is UGa_2 [10]. Having a simple hexagonal structure with one type of U site and displaying collinear ferromagnetism, it could be a "simple" reference case. However, a significant computational effort was needed to explain the large ordered uranium moments of 3.0 μ_B and the low Sommerfeld coefficient of electronic heat capacity $\gamma = 10\,\mathrm{mJ\,mol^{-1}\,K^{-2}}$ [11,12]. The Fermi surface topology, revealed by de Haas–van Alphen studies [13], could not be so far understood in any of the plausible frameworks, namely, $5f^2$ or $5f^3$ localized or $5f$ band states.

A similar seemingly simple situation is offered by U binary hydrides, which are, to a large extent, an equivalent of a volume expanded elemental uranium, with H-1s states contributing to bonding. This is the case of the metastable

*havela@matfyz.cuni.cz
†kolorenc@fzu.cz

α-UH_3 phase, equivalent to the bcc structure of γ-U expanded by 60% [14]. The stable form, β-UH_3, has a larger unit cell with two different U sites [15]. Interesting facts have been revealed by analyses of bonding and its implications on magnetism. It became apparent that the U-H bonding is based on the hybridization of H-1s states mainly with U-6d states and on charge transfer from U to H [16,17]. This may contribute to high Curie temperatures and stable U magnetic moments at relatively short U-U spacings, reaching below the Hill limit, that is, into the nonmagnetic side of the landscape of U compounds (at least for β-UH_3). A key issue is whether the electron-electron correlations are prominent in such situations or if the hydrides are simple band magnets, analogous to, e.g., transition metals. The understanding of the photoelectron spectra can play a key role in resolving this question.

The first valence-band photoemission data on UH_3 obtained on a cleaved massive sample prepared by hydrogenation at high temperatures and pressures shows the 5f states detached from the Fermi level, which would mean a substantial localization [18]. However, the level of oxygen contamination is not mentioned in [18] and as the data are reminiscent of UO_2, they have to be taken with caution. Surface reactivity of hydrides, particularly strong for actinides, is one of the important challenges of their photoemission studies. Apparently much cleaner surfaces could be obtained on *in situ* synthesized films, which was attempted in [19], revealing that there is actually a lot of 5f spectral emission close to the Fermi level. Those data were corroborated by a further development, based on improving the energy resolution and *off situ* structure studies [20,21], which identified that besides β-UH_3 one can, depending on the conditions of the synthesis, also prepare metastable UH_2 [22] not known from the U-H phase diagram, which has photoemission spectroscopy (PES) spectra very similar to the trihydride.

The aim of the present study is to present more results of x-ray photoelectron (XPS) and ultraviolet photoelectron (UPS) spectroscopies and to confront them with the state-of-the-art electronic structure calculations, including the DMFT. An emphasis is put on the interpretation of photoemission features with the aid of DMFT, which is able to unequivocally identify them as arising from the $5f^2$ multiplets of the final states remaining after the photoexcitation from the $5f^3$ initial state.

II. MATERIALS AND METHODS

We use thin films of U hydrides prepared by the same system as used in [20], that is, the reactive sputter deposition method using a miniature U target (99.9 wt % purity) and an electron emitting thoriated tungsten filament stabilizing the plasma. The deposition rates were 0.01–0.1 nm/s. We used typically the U target voltage −700 V. The working gas with pressure 0.8 Pa contained 0.06 Pa of purified H_2 gas (using the Oxisorb® cartridge), the rest being purified Ar. Varying cooling conditions of the substrate and its type as well as H_2 pressure variations can toggle the product between β-UH_3 and metastable UH_2 with fcc structure type [22]. The phase identification is based on *ex situ* x-ray diffraction analysis and magnetic properties of films prepared with the same parameters [23].

Photoelectron spectroscopy studies were performed with the UV excitation (UPS), using the He II ($h\nu = 40.81$ eV) and He I ($h\nu = 21.22$ eV) spectral lines. Their difference identifies the spectral density originating from the U-5f states, as the 5f photoexcitation cross section for the latter photon energy is negligibly small, while it dominates for the higher photon energy. The energy resolution in the UPS mode is typically about 50 meV. Complementary information has been obtained from XPS, using a monochromatized Al $K\alpha$ radiation ($h\nu = 1486.6$ eV), with the combined energy resolution about 0.5 eV. The spectrometer is based on the electron energy analyzer SPECS PHOIBOS 150 MCD-9. Most of the spectroscopic data were taken at the room temperature. The few scans taken in the ferromagnetic state ($T = 77$ K) did not reveal any significant variations compared to the paramagnetic state.

To model the photoemission spectra, we employ the LDA+DMFT method in the implementation described in [24]. First, the nonmagnetic (spin-restricted) band structure calculated in the local density approximation (LDA) is represented by a tight-binding model in the basis of the maximally localized Wannier functions, and then a momentum-independent self-energy is inserted into the uranium 5f shells to capture the correlations among the 5f electrons. This DMFT self-energy is obtained by solving an auxiliary impurity model with the Lanczos method in a reduced Fock space [12,24]. Finally, the photoemission spectra are computed as appropriate linear combinations of orbital-resolved single-particle spectral densities. For further technical details of the calculations, we refer the reader to Appendix A.

III. RESULTS

As described in [20], large-scale features of XPS spectra of UH_3 are well described by fully relativistic generalized gradient approximation (GGA) calculations, which implies that such calculations capture properly the bonding trends dominated by the strong 6d-1s hybridization forming a band between 4 and 8 eV below the Fermi energy, while the 5f states remain in the vicinity of E_F as band states. In addition, the GGA binding energy of U-6p states (not shown here) and its variations between U metal and α-UH_3 fully agree with the experimental data.

The situation within 12 eV below the Fermi level is shown in Fig. 1, which includes also historical data on UD_3 [18]. As indicated by their comparison with partly oxidized UH_3, the relevance of the UD_3 data is questionable since they exhibit mainly features attributed to UO_2, while no quantification of O was disclosed in [18]. We can therefore conclude that within the energy resolution of XPS (≈0.4 eV), the energies of 5f states are similar between U metal and UH_3. One can also see that the spectrum of UH_2 is very similar to UH_3.

There is, however, a difference in intensity which systematically decreases with increasing H concentration. The computations indicate that the 5f occupancy remains very similar ($n_{5f} \approx 2.7$); the intensity decrease can be qualitatively understood as due to the much lower density of the hydrides, reducing the number of U ions in the information depth of XPS.

The energy resolution of XPS does not allow us to decide whether the outcome of the GGA calculations, revealing the

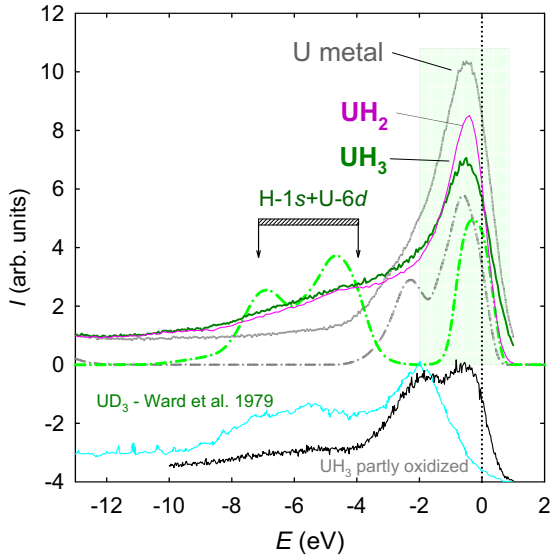

FIG. 1. Comparison of valence-band XPS spectra of elemental U (gray), UH_2 (magenta), and UH_3 (dark-green) films with results of fully relativistic GGA calculations [16] (for U and UH_3, dash-dotted) modified by the Fermi-Dirac statistics and experimental resolution. At the bottom, historical spectra of UD_3 [18] and of partly oxidized UH_3 films provide insight into the challenging process of obtaining oxygen-free surfaces. Reprinted with permission from [32].

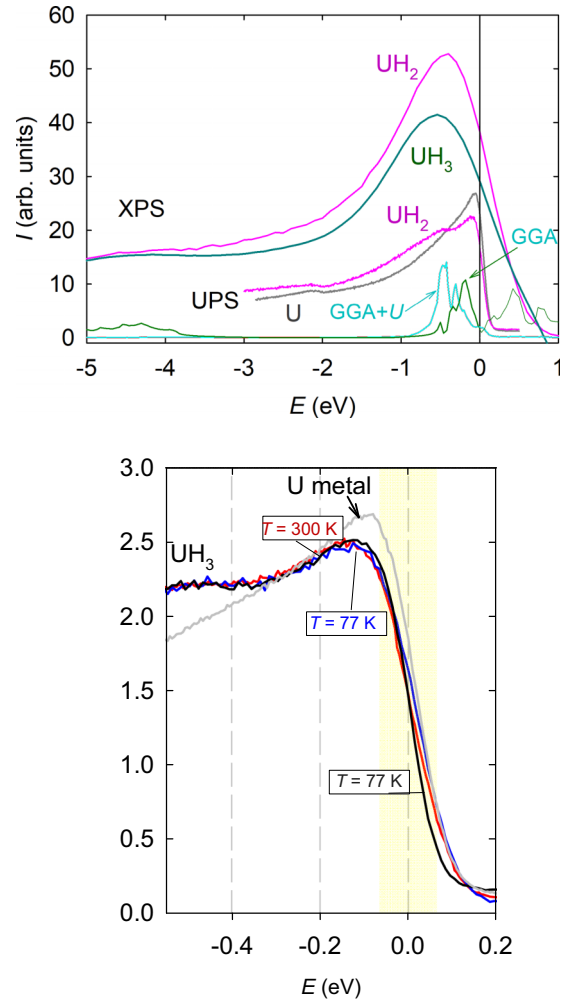

FIG. 2. Valence-band XPS and UPS (He II) photoelectron spectra of UH_3 and UH_2 compared with GGA and GGA + U calculations mentioned in the text (top). The UPS spectra of UH_3 are very similar to UH_2. The UPS spectrum of U metal is given for comparison. Details of He II UPS spectra of UH_3 (bottom) demonstrating that the spectra do not vary between the paramagnetic ($T = 300$ K; red) and ferromagnetic (77 K; blue) states. The spectrum with enhanced energy resolution at $T = 77$ K (black) has the reduced Fermi level broadening visible only above the Fermi level. The maximum located at 120 meV below the Fermi level is not affected by the Fermi-Dirac broadening with given spectrometer energy resolution, marked by the yellow rectangle. The spectrum of elemental U for the same temperature and energy resolution (gray) exhibits a monotonous increase up to the Fermi level cutoff, forming a maximum at 90–100 meV. The comparison demonstrates that the U hydride has the dominant feature separated from the Fermi level.

Fermi level near a local minimum of the density of states and the 5f band edge starting only 0.1–0.2 eV below the Fermi level (see Fig. 2), is realistic or not. The reduced density of states (DOS) at the Fermi level can help to understand the very high (for a metal) electrical resistivities, reaching 600 $\mu\Omega$ cm [18], but it apparently contradicts the enhanced Sommerfeld coefficient $\gamma = 33.9\,\mathrm{mJ\,mol^{-1}\,K^{-2}}$ [18], which is tripled compared to that of α-U.

The high-resolution UPS spectra in Fig. 2, which in principle could distinguish such a DOS minimum, offer, however, an entirely different picture. The intensity, which is dominated by the emission from the 5f states for the photon energy 40.81 eV (He II spectra), increases when approaching the Fermi energy. Unlike the U metal, the increase exhibits a shoulder at 0.5 eV followed by an additional increase up to the Fermi level. The shoulder could be in principle associated with the high DOS found in this energy range by GGA + U calculations, but the high intensity close to E_F has no explanation, neither in GGA + U nor in GGA. This disagreement is striking particularly in the case of GGA + U, which otherwise reproduces basic lattice and electronic properties of U hydrides very well, including details such as ferromagnetism, the size of U moments, equilibrium volumes, or bulk moduli [17]. A detailed view of the situation around the Fermi level (Fig. 2, bottom panel) indicates that the maximum is not formed by a density of states ascending with increasing energy (as in elemental U), which would be cut by the Fermi-Dirac statistics. It is actually located at ≈120 meV, that is, below the reach of the Fermi-Dirac broadening.

The situation changes when the Coulomb repulsion among the 5f electrons is modeled in the DMFT instead of the static mean-field (DFT + U) approximation. These calculations yield a spectral function that characterizes a reaction of the system to a photoexcitation event and that can be directly compared with photoemission spectra, which are not necessarily reflecting the ground-state density of states obtained in DFT and DFT + U methods.

The comparison of the experimental UPS and bremsstrahlung isochromat spectroscopy (BIS) [20] to the LDA + DMFT spectra of the paramagnetic phase of α-UH_3 in Fig. 3 indicates that the calculations place the uranium 5f

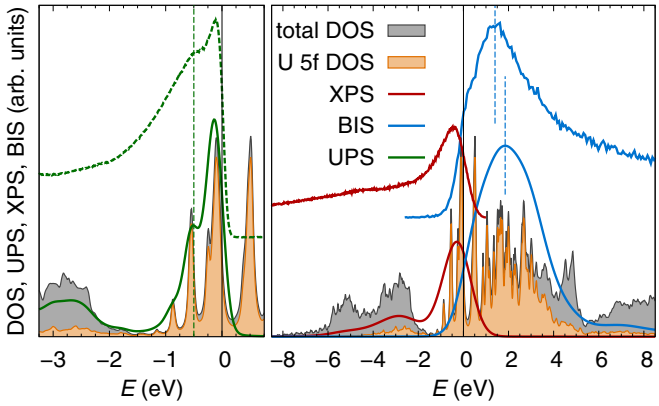

FIG. 3. Valence-band spectra for the paramagnetic phase of α-UH_3 computed with LDA + DMFT are compared with the experimental spectra: UPS (photon energy 40.81 eV), XPS (photon energy 1486.6 eV), and BIS [20]. The experimental spectra are shifted up along the vertical axis for clarity. The theoretical spectra are constructed as linear combinations of the orbital-resolved spectral densities (denoted as DOS) weighted with appropriate photoionization cross sections [43]. Gaussian broadening with FWHM 0.27 eV (UPS) and 1.3 eV (XPS and BIS) is applied to the theoretical spectra to model the instrument resolution. Reprinted with permission from [32].

states at the correct energies. Moreover, the theory reproduces the shoulder at 0.5 eV binding energy resolved in UPS, which is found to be due to a particular $5f^3 \rightarrow 5f^2$ multiplet transition. We rationalize this assignment by analyzing the DMFT impurity model with the hybridization between the $5f$ states and the other electronic states varied from zero (the atomic limit where the $5f^N \rightarrow 5f^{N-1}$ multiplet transitions are exact) to the realistic UH_3 strength. In Fig. 4 we show how the multiplet transitions continuously transform from the atomic limit to the features seen in Figs. 2 and 3. The 0.5 eV shoulder evolves from the first exited state of the $5f^2$ manifold ($^3F_2$) as hypothesized earlier [19,25].

There are several types of the photoemission final states possible in the DMFT impurity model: (i) $5f^2$ multiplets combined with the unperturbed environment (bath), (ii) $5f^2$ multiplets with electron-hole pair(s) present in the bath, and (iii) $5f^N$ multiplets with some electrons transferred from/to the bath (and possibly also combined with electron-hole pairs in the bath). In our approximate impurity model containing only a small number of bath orbitals, all these final states are discrete. In reality, the environment has a continuous spectrum and hence also the final states of the types (ii) and (iii) form a continuum. The states of the type (i) remain discrete in the sense that they become resonances in the continuum of the states (ii) and (iii).

It is perhaps surprising that even with Hubbard U as small as 1 eV, the features of atomic origin are still visible in a solid. However, the $5f$ band width is also small: in the nonmagnetic LDA or GGA calculations, the partially occupied $5f_{5/2}$ bands are only 0.5 eV wide, and the empty $5f_{7/2}$ bands are 0.75 eV wide. In the single-band Hubbard model, the metal-insulator transition takes place when the Hubbard U is slightly larger than the band width [26] and a similar phenomenon occurs also for the $5f$ states in UH_3. A subset of the multiplet features

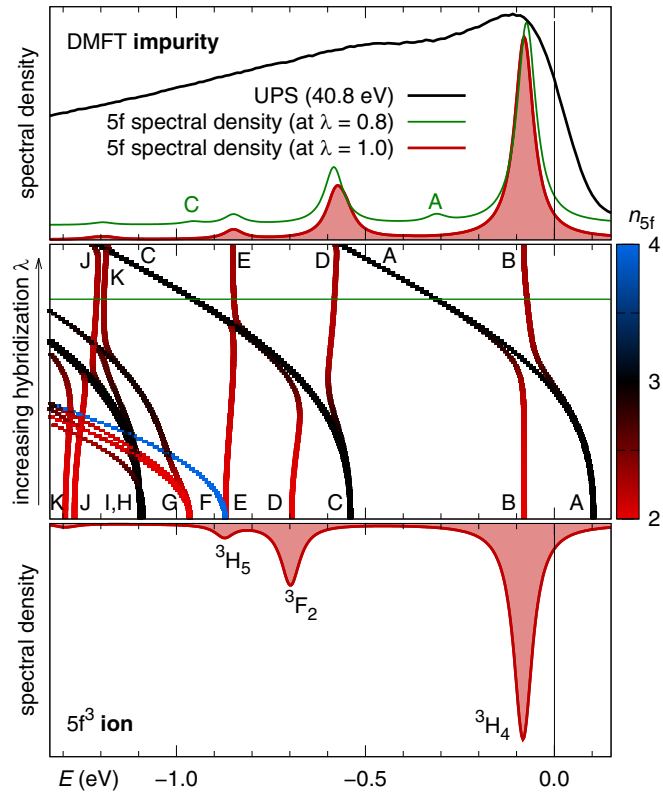

FIG. 4. Valence-band photoemission spectrum computed in the DMFT impurity model when the hybridization of the $5f$ states with their environment is varied from zero ($\lambda = 0$, atomic limit; bottom panel) to the realistic strength determined by LDA + DMFT ($\lambda = 1$; top panel). See Appendix A for the definition of the impurity model and the hybridization strength λ. The middle panel shows the evolution of the photoemission final states color-coded by their $5f$ filling (red for 2.0, black for 3.0, and blue for 4.0). In the atomic limit, the individual states are straightforward to identify: states B, D, E, J, and K are $5f^2$ multiplets (the Russel-Saunders designations shown in the figure are only approximate, since the spin and orbital moments are not good quantum numbers in uranium); states A, C, H, and I are $5f^3$ multiplets accompanied with a hole in the effective medium, state F is a $5f^4$ multiplet with two holes in the effective medium, and state G is a $5f^2$ multiplet with an electron-hole pair in the effective medium. Once the hybridization is introduced ($\lambda > 0$), these states start to mix but we can still associate the original labels with them (apart from areas near avoided crossings). In the atomic limit, only the simple $5f^2$ multiplets with no excitation in the effective medium are active in the photoemission, and these states remain dominating the photoemission spectrum up to the realistic hybridization strength. At this strength, the features A and D (as well as C and K) accidentally overlap. To visualize the intensity of features A and C, the photoemission is plotted also for a weaker hybridization ($\lambda = 0.8$; green line, vertically offset for clarity).

discussed above would collapse together and form the upper and lower Hubbard bands if the Slater parameters F_2, F_4, and F_6, responsible for the Hund's exchange and other phenomena, were removed and only the Hubbard $U = F_0$ was kept nonvanishing. For an isolated $5f^3$ ion, this collapse is illustrated in Fig. 5. It shows a model containing just the Hubbard U and spin-orbit coupling, in which the $5f^3$ ground state is a

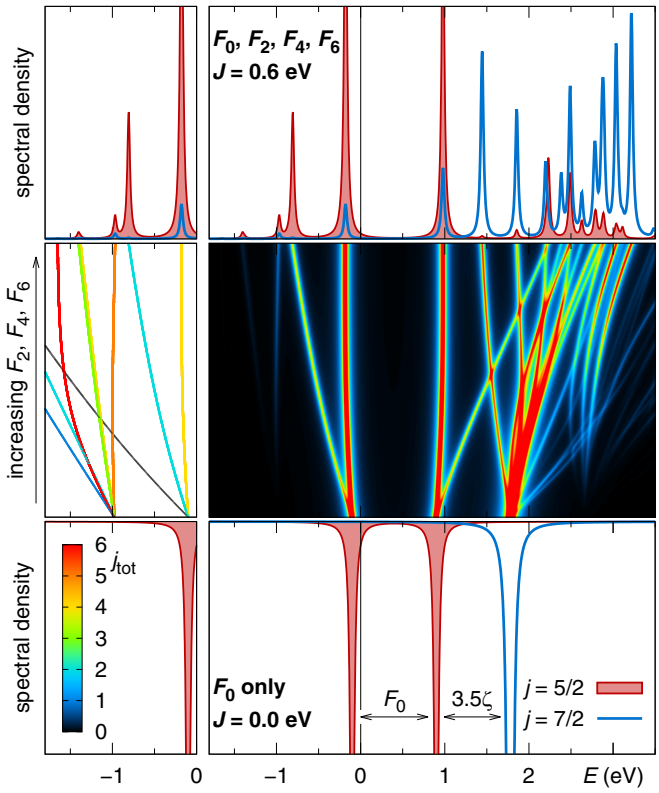

FIG. 5. Splitting of the spectral features in the $5f^3$ ion due to Slater parameters F_2, F_4, and F_6. The spectral density (decomposed into the $j = 5/2$ and $j = 7/2$ components) corresponding to vanishing F_2, F_4, and F_6 (Hund $J = 0$ eV) is shown in the bottom panels and the spectral function corresponding to the realistic values ($J = 0.6$ eV) is shown in the top panels. The middle panels illustrate the interpolation between these two limits analogously to Fig. 4: the photoemission final states, color-coded according to their total angular momentum j_{tot}, are plotted on the left, and the evolution of the spectral density is indicated as a heat map on the right. The spectral density at $F_2 = F_4 = F_6 = 0$ is particularly simple; the $j = 5/2$ level is split into two peaks separated by the Hubbard $U = F_0$; the $j = 7/2$ level is then 3.5ζ above the upper $j = 5/2$ peak, where ζ is the strength of the spin-orbit coupling (Appendix A).

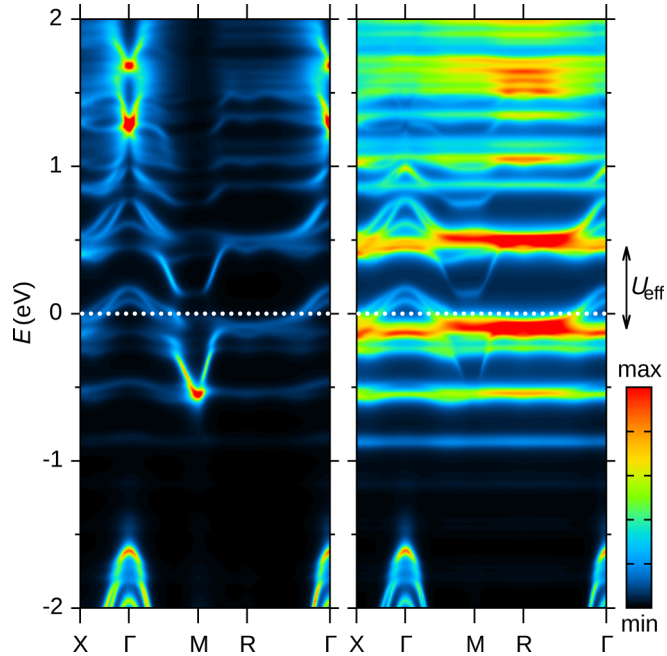

FIG. 6. LDA + DMFT band structure (Bloch spectral function) projected onto the uranium 5f states (right) and onto all other states (left). The effective (screened) Hubbard parameter U_{eff} that splits the half-filled $5f_{5/2}$ states into two Hubbard bands is indicated next to the figure.

half-filled $j = 5/2$ subshell. The spectral density displays two peaks of $j = 5/2$ character that would broaden into a lower and upper Hubbard band if the hybridization was included. Above the upper $j = 5/2$ peak, a peak of $j = 7/2$ character is located that corresponds to the empty $j = 7/2$ subshell. When the parameters F_2, F_4, and F_6 are introduced, each Hubbard band splits into three features corresponding to the final states with the total angular momentum j_{tot} equal to 4, 2, and 0 (these final states are $5f^2$ in the lower Hubbard band and $5f^4$ in the upper Hubbard band). In the lower Hubbard band, the $j_{tot} = 4$ state ($^3H_4$) becomes the main peak seen in the photoemission, the $j_{tot} = 2$ state ($^3F_2$) becomes the shoulder at 0.5 eV binding energy, whereas the $j_{tot} = 0$ state does not contribute any intensity to the spectral density. Tracking the splitting of the upper Hubbard band is intricate due to overlaps with many other spectral features, but the $j_{tot} = 4$ state ($^5I_4$) remains located approximately $U = F_0 = 1$ eV above the main peak ($^3H_4$) split off from the lower Hubbard band. An ionic spectrum like this is known from elemental Nd but with a much larger separation between the $^3H_4$ and $^5I_4$ features [27].

When the $5f^3$ ion hybridizes with the other electronic states in UH_3, the angle-integrated 5f spectrum is still quite close to the ionic spectrum as was demonstrated in Fig. 4. A more detailed view on the electronic structure is provided by the momentum-resolved spectrum plotted in Fig. 6, where we compare the Bloch spectral function projected onto the 5f states and onto all other states included in our LDA + DMFT calculation. The separation between the main components of the 5f Hubbard bands, the $^3H_4$ and $^5I_4$ features, is reduced to $U_{eff} \approx 0.6$ eV indicating a sizable screening of the Coulomb interaction, which is discussed also in Appendix A. The 5f Hubbard bands hybridize with dispersive bands (of mainly uranium 6d character) and the resulting dispersive hybrid bands make the system metallic as they cross the Fermi level, at which point their composition is 80% 5f states and 20% the rest of states.

Qualitatively, the Hubbard U and the other Coulomb parameters push the 5f electrons toward the strongly correlated regime; the hybridization with the dispersive bands has the opposite effect. One possible quantitative measure of the 5f correlations is the valence histogram $P(N)$, which visualizes how the 5f shell fluctuates between individual $5f^N$ configurations [7,28] and which carries an analogous information as the double occupancy does in the single-band Hubbard model [26]. The width of the histogram also reflects the degree of localization of the 5f electrons. A more localized 5f shell fluctuates less and the corresponding histogram is narrower. However, one should not expect that localized 5f states (beyond Am in elemental actinides) do not fluctuate at all just as

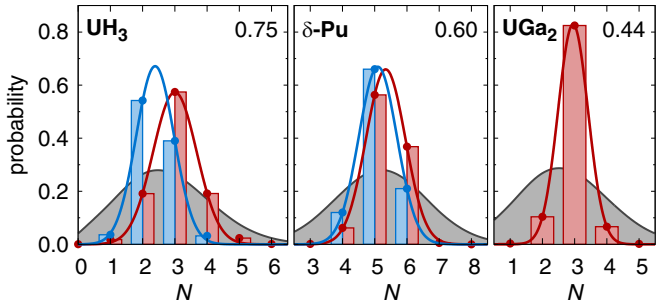

FIG. 7. Valence histogram for the $5f$ states in UH_3 is compared to the situation in δ-Pu and UGa_2. The narrower the histogram, the more correlated (and presumably more localized) the $5f$ electrons are. The colored lines are fits with the Gaussian distribution, the black lines represent a distribution corresponding to the uncorrelated electrons (see Appendix B), and the numbers shown in the top right corners are fluctuations of the $5f$ filling, that is, the square root of the variance of the corresponding histogram. The red data were obtained from DMFT calculations analogous to the present study (the histogram for δ-Pu corresponds to [8] and the histogram for UGa_2 corresponds to [12]), and the blue data for UH_3 are taken from [30] and for δ-Pu from [29], where a different impurity solver (continuous-time quantum Monte Carlo) was used.

the double occupancy in the Hubbard model does not entirely vanish in the Mott insulator phase [26].

Figure 7 compares the valence histogram of UH_3 with histograms of δ-Pu [8,29] and UGa_2 [12]. The UH_3 histogram being wider than the δ-Pu histogram is a sign that at least some of the $5f$ electrons in UH_3 are delocalized, since the $5f$ shell in δ-Pu is at the borderline between the localized and the itinerant character. The $5f$ electrons in UH_3 are the least correlated of the three substances but they are still far from the uncorrelated limit that is also indicated in Fig. 7. The valence histogram reported for α-UH_3 in [30] (and also shown in Fig. 7) is narrower than ours and it alternatively suggests that the correlations in UH_3 could be roughly comparable to δ-Pu.

There are many similarities between our study and [30] since both are applications of the LDA + DMFT method, but there are also several important differences (different impurity solver, different double-counting scheme, or different Coulomb parameters). The larger Hubbard U (5.3 eV instead of our 1.0 eV) is the likely reason for the narrower valence histogram as a larger U naturally suppresses the local charge fluctuations and pushes the $5f$ electrons toward localization. The different double-counting scheme is probably responsible for the lower filling of the $5f$ shell found in [30] (2.4 instead of our 3.0), which in turn could be the cause for the strongly reduced DOS feature at the 0.5-eV binding energy, although some smearing effect of the analytical continuation employed in [30] cannot be entirely excluded either. What is quite puzzling, however, is the gap between occupied and unoccupied $5f$ states found in [30] being comparable to the gap found in our calculations (Figs. 3 and 6) despite the much larger Hubbard U. When we increase U, the unoccupied $5f$ states move up in energy and would end up several eV higher than shown in Figs. 3 and 6 if we set $U = 5.3$ eV. Apparently, a considerably more efficient screening of the Coulomb repulsion is predicted in [30] when the unoccupied $5f$ states remain much closer to the Fermi level even with the much larger U. Such large screening appears incompatible with our present findings and past experience (see also Appendix A).

IV. DISCUSSION

The multiplet structure appearing in the valence-band spectra is undoubtedly a fingerprint of strong electron-electron correlations, arising gradually in $5f$ band systems as the bandwidth is reduced. A semiquantitative estimate of the band width before explicit correlations are triggered can be done, e.g., on the basis of spin-polarized GGA calculations of α-UH_3 (with spin-orbit coupling included), in which the dominant portion of the $5f$ states falls for each spin subband into the energy range ≈ 2 eV wide [16]. Using the same method, the non-spin-polarized band of U metal (weakly correlated Pauli paramagnet) gives about 4 eV bandwidth, so the effect of volume expansion and polar bonding is substantial. A primary effect of correlations is naturally the ferromagnetism of U hydrides. The size of the U moments, approximately 1 μ_B, is by far too small in comparison with localized f^2 or f^3 states (3.20 and 3.27 μ_B, respectively, in the L-S coupling scheme). Moreover, a sizable spontaneous magnetostriction, that is, an increase of the volume in the ferromagnetic state, is suggestive of additional spin splitting induced in the ordered state [31]. Such invar effect is attributed to the band character of magnetism. The γ coefficient in the paramagnetic state, increasing to 60 mJ mol^{-1} K^{-2}, is only the other side of the same coin [32]. Last but not least, the pressure decrease of T_C indicates that the magnetism of UH_3 is essentially coming from the $5f$ band, but its moderate pressure or volume derivatives reveal that the band picture is not the whole story and a partial $5f$ localization has to be admitted [33].

The fact that the LDA + DMFT calculations provide full understanding of the valence-band photoelectron spectra of U hydrides in terms of the $5f^2$ multiplets can be taken as a positive fact. However, it means that important fine details of the band structure remain inaccessible for the spectroscopy. In particular, standard angle-integrated photoelectron spectroscopy cannot help to decide if the hydrides are metals, semimetals, or perhaps half metals. Angle-resolved photoemission, which can better isolate the almost dispersionless states, derived from atomic multiplets, from dispersive band states, could be instrumental, but hydrides generally allow crystal synthesis only very seldom. The question naturally is, how much the atomic excitations affect also spectra of other uranium or generally actinide systems. The case of Pu systems, mentioned in the Introduction, indicates their dominance over a broad range spanning various regimes. The mapping for U-based systems has to be still undertaken. The message for now is that confrontation of first-principles calculations with photoelectron spectra has to be done with caution since the spectra can be dominated by features not derived from the ground-state density of states even in the absence of $5f$ localization. The type of valence-band spectra with the 0.5 eV satellite can be hence quite generic and not material specific. As an example, the PES spectra (at least the angle-integrated ones) of U hydrides are very similar to those

of UTe_2 reported in [34]. We consider this similarity to be worth exploring in more detail in the future.

V. CONCLUSIONS

We found that the high-resolution UPS spectra of UH_3 can be understood as reflecting the $5f^2$ multiplets of final states that remain after the photoexcitation from the $5f^3$ initial state. Other configurations are present as well, although their participation is relatively minor. The example of U hydrides hence gives an indication that the final-state multiplets in PES may be quite common even in situations when the $5f$ band picture is an appropriate starting point for the description of the ground state. The general message is that the link between spectra and the ground-state density of states is only indirect, and the spectra cannot be simply used to corroborate the results of DFT or DFT + U calculations.

ACKNOWLEDGMENTS

The work has been supported by the Czech Science Foundation under Grant No. 21-09766S. The experimental data used in this research were generated through access to the ActUsLab/PAMEC under the Framework of access to the Joint Research Centre Physical Research Infrastructures of the European Commission (HYDROFILM_1, PAMEC Access Agreement No. 35630, AUL-2018-21-214, POLAR_-2021, AUL-2020-23-224, No. 36107/04, and No. UTFilm_1, AUL-2020-23-227, No. 36107/11). Computational resources were provided by the e-INFRA CZ project (ID 90254), supported by the Ministry of Education, Youth and Sports of the Czech Republic.

APPENDIX A: DETAILS OF THE LDA + DMFT CALCULATIONS

The starting LDA band structure is calculated using WIEN2K software [35] and includes scalar relativistic effects as well as spin-orbit coupling. The subsequent tight-binding model is constructed with the aid of the WANNIER90 code [36,37] and contains uranium $5f$, $6d$, $7s$, $7p$, and hydrogen $1s$ states. This basis allows for an accurate representation of the original LDA band structure in the energy window from -10 to 7 eV around the Fermi level; higher-lying bands are represented only approximately.

To lower the computational complexity, the DMFT auxiliary impurity model is constrained to be spherically symmetric. Our tests indicate that including the nonspherical terms would lead to a splitting of the individual photoemission features (multiplets) that would be much smaller than their spacing. The impurity Hamiltonian takes the form

$$H_{\mathrm{imp}} = \sum_{j,n} h_j^{\mathrm{loc}} f_{jn}^\dagger f_{jn} + \sum_{k,j,n} \epsilon_{kj} b_{kjn}^\dagger b_{kjn} + \lambda \sum_{k,j,n} V_{kj} (f_{jn}^\dagger b_{kjn} + b_{kjn}^\dagger f_{jn}) + H_{\mathrm{Coul}}, \quad \text{(A1)}$$

where $j \in \{5/2,\ 7/2\}$, $n \in \{-j, \ldots, j\}$, and $k \in \{1, 2, 3\}$. Operator $f_{jn}^\dagger$ creates an electron in the $5f$ shell and operator $b_{kjn}^\dagger$ creates an electron in the effective medium (bath). The same size of the impurity model (42 bath orbitals) was used in our earlier investigations of metallic actinide systems: δ-Pu [8] or UGa_2 [12]. The local Hamiltonian of the $5f$ shell h_j^{loc} contains the spin-orbit coupling term $\zeta(\boldsymbol{l}\cdot\boldsymbol{s})$ with $\zeta = 0.25$ eV found directly from the tight-binding model; the parameters describing the hybridization of the $5f$ shell with the effective medium, ϵ_{kj} and V_{kj}, are determined by fitting the bath Green's function at the Matsubara frequencies (the first 200 Matsubara frequencies were included in the fit; the temperature was set to 160 K) [26,38]. The scaling factor λ is equal to 1 in the standard LDA + DMFT calculation, and it is varied from 0 to 1 to interpolate from the atomic limit to the DMFT solution in Fig. 4.

The Coulomb interaction in the $5f$ shell, H_{Coul}, is considered in its full spherically symmetric form parametrized by four Slater integrals $F_0 = 1.0$ eV, $F_2 = 7.09$ eV, $F_4 = 4.60$ eV, and $F_6 = 3.36$ eV, which correspond to Hubbard $U = 1.0$ eV and Hund $J = 0.59$ eV. The first integral, $F_0 = U$, is chosen to get the gap between the occupied and unoccupied $5f$ states compatible with the GGA + U calculations reported in [17] and with the XPS and BIS spectra. The other three parameters (F_2, F_4, F_6) correspond to the atomic Hartree-Fock values calculated for the U^{3+} ion ($5f^3$ configuration) and then reduced to 80% to simulate screening and multiconfigurational effects [39,40]. The double-counting correction is implemented in the fully localized limit, $U_{\mathrm{DC}} = U(n_{5f} - 1/2) - J(n_{5f} - 1)/2 = 1.7$ eV, where $n_{5f} = 2.72$ is the LDA filling of the $5f$ Wannier orbitals.

Our Hubbard $U = 1.0$ eV is twice as large as U used in the earlier GGA + U calculations [17]. It is a general property of the DFT + DMFT method that it requires larger values of the $5f$-$5f$ Coulomb interaction parameters than the DFT + U method to yield comparable results as discussed elsewhere [12,24]. Previously, 1.3 times larger U was needed in UGa_2 [12] and approximately two times larger U was needed in UO_2 [24] to obtain the same gap between occupied and unoccupied $5f$ states.

In the impurity model corresponding to the converged DMFT solution, there are 22 bath orbitals (one $j = 5/2$ subshell and two $j = 7/2$ subshells) below the Fermi level (nominally filled) and 20 bath orbitals (two $j = 5/2$ subshells and one $j = 7/2$ subshell) above the Fermi level (nominally empty). We employ a Fock-space truncation to reduce the computational demands of the impurity solver. It amounts to limiting the number of deviations M from the nominal occupations of the bath orbitals [12,24]. In the DMFT iterations (i.e., for calculating the one-particle Green's function) we set $M = 3$ and for the explicit calculation of the $5f^2$ final states in Fig. 4 we use a smaller Fock space defined by $M = 2$.

It is expected that the more itinerant the $5f$ electrons are, the larger M is required. Previously, we have demonstrated that $M = 2$ already gives essentially converged total energies and $5f$ fillings in UGa_2 with quite localized $5f$ states [12]. The valence histogram of δ-Pu shown in Fig. 7 was computed with $M = 3$ [8] and its close similarity to the valence histogram found with a continuous-time quantum Monte Carlo impurity solver [29] implies that the $M = 3$ Fock space is sufficient for δ-Pu. In the case of UH_3, $M = 3$ should also represent an accurate approximation even though the $5f$ electrons are slightly more delocalized than in δ-Pu (Fig. 7). A direct

test of the convergence by setting $M = 4$ cannot be performed as such calculations are simply too demanding at present.

APPENDIX B: VALENCE HISTOGRAM FOR UNCORRELATED 5f ELECTRONS

The valence histogram for the uncorrelated electrons can be calculated from the DFT wave function, that is, from the Slater determinant of Kohn-Sham orbitals [28,41]. In Fig. 7, we use a cheaper alternative, an estimate based on simple combinatorics [42]: If there are n electrons in a shell on average, the probability of finding an electron in each of its orbitals is $p = n/M$, where M is the degeneracy of the shell. Uncorrelated electrons jump to and from the shell independently of each other, which means that the probability to find N electrons in the shell is given by the binomial distribution

$$B(p, M; N) = \binom{M}{N} p^N (1-p)^{M-N},$$

the variance of which is $Mp(1-p)$, that is, the fluctuations are largest for a half-filled shell and are very small for nearly empty or nearly full shells.

The reasoning leading to the binomial distribution assumes that all 5f orbitals are equivalent, which is not entirely true, since the crystal field, spin-orbit coupling as well as non-isotropic hybridization break this equivalency. To improve the estimate, we take the spin-orbit splitting into account and allow different probabilities for the $j = 5/2$ subshell, $p_{5/2} = n_{5/2}/M_{5/2}$, and for the $j = 7/2$ subshell, $p_{7/2} = n_{7/2}/M_{7/2}$.

TABLE I. Occupations of the $j = 5/2$ and $j = 7/2$ 5f subshells computed in the nonmagnetic LDA solution as fillings of the corresponding maximally localized Wannier functions, and DMFT probabilities $P(N)$ of finding N electrons in the 5f shell (the same data are visualized in Fig. 7).

		α-UH_3	UGa_2	δ-Pu
LDA	$n_{5/2}$	2.03	2.24	4.29
	$n_{7/2}$	0.69	0.48	0.91
DMFT	$P(1)$	0.018	0.033	
	$P(2)$	0.191	0.104	
	$P(3)$	0.574	0.825	0.002
	$P(4)$	0.192	0.066	0.062
	$P(5)$	0.024	0.002	0.563
	$P(6)$	0.001		0.368
	$P(7)$			0.005

Then the probability distribution $P(N)$ reads as

$$P(p_{5/2}, M_{5/2}, p_{7/2}, M_{7/2}; N) = \sum_{N_{5/2}=0}^{\min(N, M_{5/2})} B(p_{5/2}, M_{5/2}; N_{5/2}) B(p_{7/2}, M_{7/2}; N - N_{5/2}),$$

where the sum runs over all possible arrangements of N electrons in the two subshells. The variance of this distribution is $M_{5/2}p_{5/2}(1-p_{5/2}) + M_{7/2}p_{7/2}(1-p_{7/2})$. For the uncorrelated histograms shown in Fig. 7, we take $n_{5/2}$ and $n_{7/2}$ to be the occupations of the maximally localized Wannier functions in the nonmagnetic LDA calculations (Table I).

[1] S. Ran, C. Eckberg, Q.-P. Ding, Y. Furukawa, T. Metz, S. R. Saha, I.-L. Liu, M. Zic, H. Kim, J. Paglione *et al.*, Nearly ferromagnetic spin-triplet superconductivity, Science **365**, 684 (2019).

[2] J. L. Sarrao, L. A. Morales, J. D. Thompson, B. L. Scott, G. R. Stewart, F. Wastin, J. Rebizant, P. Boulet, E. Colineau, and G. H. Lander, Plutonium-based superconductivity with a transition temperature above 18 K, Nature (London) **420**, 297 (2002).

[3] J. A. Mydosh, P. M. Oppeneer, and P. S. Riseborough, Hidden order and beyond: An experimental-theoretical overview of the multifaceted behavior of URu_2Si_2, J. Phys.: Condens. Matter **32**, 143002 (2020).

[4] H. Ott, H. Rudigier, P. Delsing, and Z. Fisk, Magnetic ground-state of a heavy-electron system: U_2Zn_{17}, Phys. Rev. Lett. **52**, 1551 (1984).

[5] H. Ott, H. Rudigier, Z. Fisk, and J. Smith, UBe_{13}: An unconventional actinide superconductor, Phys. Rev. Lett. **50**, 1595 (1983).

[6] A. Shick, J. Kolorenč, L. Havela, V. Drchal, and T. Gouder, Multiplet effects in the electronic structure of δ-Pu, Am and their compounds, Europhys. Lett. **77**, 17003 (2007).

[7] J. H. Shim, K. Haule, and G. Kotliar, Fluctuating valence in a correlated solid and the anomalous properties of δ-plutonium, Nature (London) **446**, 513 (2007).

[8] L. Havela, S. Mašková, J. Kolorenč, E. Colineau, J.-C. Griveau, and R. Eloirdi, Electronic properties of $Pu_{19}Os$ simulating β-Pu: The strongly correlated Pu phase, J. Phys.: Condens. Matter **30**, 085601 (2018).

[9] H. H. Hill, The early actinides: The periodic system's f electron transition metal series, in *Plutonium 1970 and Other Actinides*, edited by W. N. Miner (Metallurgical Society of AIME, New York, 1970), pp. 1–19.

[10] A. V. Kolomiets, J.-C. Griveau, J. Prchal, A. V. Andreev, and L. Havela, Variations of magnetic properties of UGa_2 under pressure, Phys. Rev. B **91**, 064405 (2015).

[11] A. V. Kolomiets, M. Paukov, J. Valenta, B. Chatterjee, A. V. Andreev, K. O. Kvashnina, F. Wilhelm, A. Rogalev, D. Drozdenko, P. Minarik, J. Kolorenc, M. Richter, J. Prchal, and L. Havela, 5f states in UGa_2 probed by x-ray spectroscopies, Phys. Rev. B **104**, 045119 (2021).

[12] B. Chatterjee and J. Kolorenč, Electronic structure and magnetism in UGa_2: DFT + DMFT approach, Phys. Rev. B **103**, 205146 (2021).

[13] T. Honma, Y. Inada, R. Settai, S. Araki, Y. Tokiwa, T. Takeuchi, H. Sugawara, H. Sato, K. Kuwahara, M. Yokoyama *et al.*, Magnetic and Fermi surface properties of the ferromagnetic compound UGa_2, J. Phys. Soc. Jpn. **69**, 2647 (2000).

[14] R. N. R. Mulford, F. H. Ellinger, and W. H. Zachariassen, A new form of uranium hydride, J. Am. Chem. Soc. **76**, 297 (1954).

[15] R. E. Rundle, The hydrogen positions in uranium hydride by neutron diffraction, J. Am. Chem. Soc. **73**, 4172 (1951).

[16] I. Tkach, M. Paukov, D. Drozdenko, M. Cieslar, B. Vondráčková, Z. Matěj, D. Kriegner, A. V. Andreev, N.-T. H. Kim-Ngan, I. Turek *et al.*, Electronic properties of α-UH_3 stabilized by Zr, Phys. Rev. B **91**, 115116 (2015).

[17] L. Kývala, L. Havela, A. P. Kądzielawa, and D. Legut, Electrons and phonons in uranium hydrides—effects of polar bonding, J. Nucl. Mater. **567**, 153817 (2022).

[18] J. W. Ward, L. E. Cox, J. L. Smith, G. R. Stewart, and J. H. Wood, Some observations on the electronic-structure of β-UD_3, J. Phys. Colloq. **40**, C4 (1979).

[19] T. Gouder, R. Eloirdi, F. Wastin, E. Colineau, J. Rebizant, D. Kolberg, and F. Huber, Electronic structure of UH_3 thin films prepared by sputter deposition, Phys. Rev. B **70**, 235108 (2004).

[20] L. Havela, M. Paukov, M. Dopita, L. Horák, M. Cieslar, D. Drozdenko, P. Minárik, I. Turek, M. Diviš, D. Legut *et al.*, XPS, UPS, and BIS study of pure and alloyed β-UH_3 films: Electronic structure, bonding, and magnetism, J. Electron Spectrosc. Relat. Phenom. **239**, 146904 (2020).

[21] E. A. Tereshina-Chitrova, L. Havela, M. Paukov, M. Dopita, L. Horak, O. Koloskova, Z. Soban, T. Gouder, F. Huber, and A. Seibert, Role of disorder in magnetic and conducting properties of U-Mo and U-Mo-H thin films, Mater. Chem. Phys. **260**, 124069 (2021).

[22] L. Havela, M. Paukov, M. Dopita, L. Horák, D. Drozdenko, M. Diviš, I. Turek, D. Legut, L. Kývala, T. Gouder *et al.*, Crystal structure and magnetic properties of uranium hydride UH_2 stabilized as a thin film, Inorg. Chem. **57**, 14727 (2018).

[23] E. A. Tereshina-Chitrova, L. Havela, M. Paukov, O. Koloskova, L. Horák, M. Dopita, M. M. Celis, M. Cieslar, Z. Šobáň, T. Gouder *et al.*, Synthesis and physical properties of uranium thin-film hydrides UH_2 and UH_3, Thin Solid Films **775**, 139860 (2023).

[24] J. Kolorenč, A. B. Shick, and A. I. Lichtenstein, Electronic structure and core-level spectra of light actinide dioxides in the dynamical mean-field theory, Phys. Rev. B **92**, 085125 (2015).

[25] T. Gouder, A. Seibert, J. Rebizant, F. Huber, and L. Havela, Comparative photoemission study of actinide (Am, Pu, Np and U) metals, nitrides, and hydrides, MRS Proc. **986**, 9860102 (2006).

[26] A. Georges, G. Kotliar, W. Krauth, and M. J. Rozenberg, Dynamical mean-field theory of strongly correlated fermion systems and the limit of infinite dimensions, Rev. Mod. Phys. **68**, 13 (1996).

[27] J. K. Lang, Y. Baer, and P. A. Cox, Study of the 4f and valence band density of states in rare-earth metals. II. Experiment and results, J. Phys. F: Met. Phys. **11**, 121 (1981).

[28] P. Fulde, *Electron Correlations in Molecules and Solids*, 3rd ed. (Springer, Berlin, Heidelberg, 1995).

[29] M. Janoschek, P. Das, B. Chakrabarti, D. L. Abernathy, M. D. Lumsden, J. M. Lawrence, J. D. Thompson, G. H. Lander, J. N. Mitchell, S. Richmond *et al.*, The valence-fluctuating ground state of plutonium, Sci. Adv. **1**, e1500188 (2015).

[30] R. Li, Y. Wan, X. Lu, J. Wang, D. Xin, and J. Zhang, Dual 5f character in two allotropes of uranium trihydride studied via a first principles calculation, Chem. Phys. **538**, 110876 (2020).

[31] L. Havela, M. Paukov, I. Tkach, Z. Matěj, D. Kriegner, S. Mašková, B. Vondráčková, M. Prachařová, I. Turek, M. Diviš *et al.*, UH_3-based ferromagnets: New look at an old material, J. Magn. Magn. Mater. **400**, 130 (2016).

[32] L. Havela, D. Legut, and J. Kolorenč, Hydrogen in actinides: Electronic and lattice properties, Rep. Prog. Phys. **86**, 056501 (2023).

[33] J. Prchal, V. Buturlim, J. Valenta, M. Dopita, M. Divis, I. Turek, L. Kyvala, D. Legut, and L. Havela, Pressure variations of the 5f magnetism in UH_3, J. Magn. Magn. Mater. **497**, 165993 (2020).

[34] S. Fujimori, D. Kawasaki, Y. Takeda, H. Yamagami, A. Nakamura, Y. Homma, and D. Aoki, Electronic structure of UTe_2 studied by photoelectron spectroscopy, J. Phys. Soc. Jpn. **88**, 103701 (2019).

[35] P. Blaha, K. Schwarz, F. Tran, R. Laskowski, G. K. H. Madsen, and L. D. Marks, WIEN2k: An APW+lo program for calculating the properties of solids, J. Chem. Phys. **152**, 074101 (2020).

[36] A. A. Mostofi, J. R. Yates, Y.-S. Lee, I. Souza, D. Vanderbilt, and N. Marzari, Wannier90: A tool for obtaining maximally-localised Wannier functions, Comput. Phys. Commun. **178**, 685 (2008).

[37] G. Pizzi, V. Vitale, R. Arita, S. Blügel, F. Freimuth, G. Géranton, M. Gibertini, D. Gresch, C. Johnson, T. Koretsune *et al.*, Wannier90 as a community code: New features and applications, J. Phys.: Condens. Matter **32**, 165902 (2020).

[38] A. Liebsch and H. Ishida, Temperature and bath size in exact diagonalization dynamical mean field theory, J. Phys.: Condens. Matter **24**, 053201 (2012).

[39] R. D. Cowan, *The Theory of Atomic Structure and Spectra* (University of California Press, Berkeley, 1981).

[40] H. Ogasawara, A. Kotani, and B. T. Thole, Calculation of magnetic x-ray dichroism in 4d and 5d absorption spectra of actinides, Phys. Rev. B **44**, 2169 (1991).

[41] F. Pfirsch, M. C. Böhm, and P. Fulde, Electron correlations in hydrocarbon molecules, Z. Phys. B **60**, 171 (1985).

[42] J. Hubbard, Electron correlations in narrow energy bands, Proc. R. Soc. London, Ser. A **276**, 238 (1963).

[43] J. J. Yeh and I. Lindau, Atomic subshell photoionization cross sections and asymmetry parameters: $1 \leqslant Z \leqslant 103$, At. Data Nucl. Data Tables **32**, 1 (1985).